

# Human-Imperceptible Physical Adversarial Attack for NIR Face Recognition Models

Songyan Xie<sup>1</sup>, Jinghang Wen<sup>2</sup>, Encheng Su<sup>3</sup>, Qiucheng Yu<sup>2\*</sup>

<sup>1</sup> School of Computer Science and Technology, China University of Mining and Technology, Xuzhou, China

<sup>2</sup> Department of Computer Science, City University of Hong Kong, Hong Kong, China

<sup>3</sup> Department of Engineering and Design, Technische Universität München, München, Germany

xiesongyan@cumt.edu.cn, jh.wen@my.cityu.edu.hk, encgo.su@tum.de, qiuchenyu2-c@my.cityu.edu.hk

## Abstract

Near-infrared (NIR) face recognition systems, which can operate effectively in low-light conditions or in the presence of makeup, exhibit vulnerabilities when subjected to physical adversarial attacks. To further demonstrate the potential risks in real-world applications, we design a novel, stealthy, and practical adversarial patch to attack NIR face recognition systems in a black-box setting. We achieved this by utilizing human-imperceptible infrared-absorbing ink to generate multiple patches with digitally optimized shapes and positions for infrared images. To address the optimization mismatch between digital and real-world NIR imaging, we develop a light reflection model for human skin to minimize pixel-level discrepancies by simulating NIR light reflection. Compared to state-of-the-art (SOTA) physical attacks on NIR face recognition systems, the experimental results show that our method improves the attack success rate in both digital and physical domains, particularly maintaining effectiveness across various face postures. Notably, the proposed approach outperforms SOTA methods, achieving an average attack success rate of 82.46% in the physical domain across different models, compared to 64.18% for existing methods. The artifact is available at <https://anonymous.4open.science/r/Human-imperceptible-adversarial-patch-0703/>.

## 1. Introduction

Face recognition models have been applied in various tasks, including surveillance [32], border security [3], and access control [1, 25]. However, traditional visible (VIS) face recognition systems encounter performance degradation under challenging conditions such as dark environments or makeup. To overcome these limitations, near-infrared (NIR) face recognition systems have emerged as

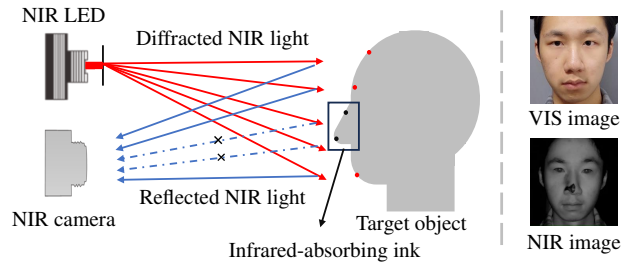


Figure 1. The diagram illustrates the theory of the NIR face recognition system and our proposed attack strategy. The left subfigure shows that infrared-absorbing ink can absorb diffracted NIR light and reduce the reflected NIR light used for imaging. The right subfigure presents our adversarial ink patch. The VIS image, perturbed with the ink, remains imperceptible, while the NIR image successfully executes an adversarial attack.

a powerful alternative, as they can capture facial features in low-light or complex environments by utilizing the unique properties of infrared light, which is immune to visible lighting and cosmetic alterations [18, 19].

Modern NIR face recognition systems leverage deep neural networks (DNNs) to extract illumination-robust features and establish cross-modal mappings between NIR and VIS images [12, 38]. While these DNN-driven architectures achieve state-of-the-art recognition accuracy, their inherent vulnerability to adversarial perturbations [30] raises critical security concerns, since a small perturbation added to the input can lead to incorrect identity judgments. Previous work has successfully achieved physical adversarial attacks on VIS face recognition systems by embedding adversarial perturbations into common accessories, such as hats [28], glasses [28], and masks [45], which mislead the system into predicting the wrong identity. Considering the concealment requirement of adversarial patches, some other works exploit imperceptible optical interference mechanisms, including infrared light illumination manipulation [33] and

\*Corresponding author

persistence-of-vision effects [29], which bypass human visual detection while compromising VIS face recognition systems. To explore the vulnerabilities of NIR face recognition systems, research [6] reveals that printable adversarial eyeglasses can effectively deceive NIR face recognition systems by minimizing color derivation between digital simulations and physical deployments in the NIR spectrum.

All the aforementioned works primarily focus on VIS face recognition adversarial attacks. Although research [6] has achieved successful attacks on NIR face recognition systems, it overlooked the stealthiness and real-world feasibility. These limitations stem from three fundamental challenges inherent to NIR face recognition systems attacks. (i) Most previous studies targeting VIS face recognition attacks cannot mislead NIR face recognition systems, as NIR images are robust to lighting-variation due to specialized wavelength filters and exhibit lower dimensionality correlating with reduced susceptibility to attacks [27]. (ii) Some other works generated perturbations in NIR images, but the strange patch patterns appeared significantly suspicious in the VIS environment, which fails to meet the concealment needs for attacks. (iii) The only study [6] that conducted a white-box attack on the NIR face recognition model, which requires complete knowledge of the model’s structure and parameters, conflicts with real-world deployments black-box constraints where only the model’s predicted label and probability are accessible.

To address the above challenges, we propose a novel human-imperceptible physical adversarial patch designed to deceive NIR face recognition systems. As illustrated in Fig. 1, our method employs transparent infrared-absorbing ink to generate a human-imperceptible adversarial patch that effectively disrupts NIR facial imaging. Furthermore, we introduce a comprehensive attack framework that jointly optimizes the shapes and positions of patches under strictly black-box settings. By simulating NIR light reflection during optimization, our patch is refined to achieve the physical optimal shape and position, resulting in an average attack success rate of 82.46% across different models in the physical domain, compared to 64.18% for the existing state-of-the-art method.

Our main contributions are summarized as follows.

- To achieve a stealthy and effective adversarial attack for NIR face recognition systems, we propose the first human-imperceptible physical adversarial patch utilizing infrared-absorbing ink. This method ensures the patch is imperceptible in the VIS spectrum while effectively misleading NIR face recognition models.
- To optimize the patch under strict black-box conditions, we develop a multi-patch adversarial attack framework. This framework jointly optimizes patch shape and position relying on model prediction labels

and probabilities, eliminating the need for white-box access and enhancing real-world applicability.

- To bridge the gap between digital simulation and real-world NIR imaging, we introduce a light reflection model that simulates NIR light reflection with human skin. This model guides the optimization process toward the physically optimal patch configuration, ensuring its effectiveness after physical deployment.

## 2. Background and Related Work

In this section, we first provide an overview of NIR face recognition systems, followed by a review of existing adversarial attacks in both the digital and physical domains.

### 2.1. Face Recognition in NIR

Near-infrared (NIR) refers to light in the electromagnetic spectrum, with wavelengths ranging from 750 nm to 1400 nm. While existing research predominantly focuses on the visible spectrum face recognition systems, the integration of NIR imaging significantly enhances robustness against pose variations, illumination changes, and partial occlusions, owing to NIR’s inherent insensitivity to visible lighting fluctuations and cosmetic alterations [13]. Additionally, the reflection difference between live spoof faces under NIR can be exploited to detect presentation attacks such as print, video replay, makeup, and 3D mask [16]. These advantages have led to the security-critical adoption of NIR face recognition systems *e.g.*, [1, 25].

Leading NIR face recognition systems rely on DNNs[11, 39, 12, 14, 24, 38]. For example, Wu *et al.* proposed the LightCNN framework, designed for deep face representation using large-scale datasets with noisy labels, which was optimized for efficiency and adaptability across various face recognition tasks [38]. Based on this, Fu *et al.* introduced LightCNN-DVG [11], which achieved state-of-the-art performance in NIR face recognition. The key innovation of LightCNN-DVG lies in its fine-tuning process with NIR-VIS data, ensuring identity consistency through distribution alignment in the latent space and pairwise identity preservation in the feature space while mapping features of different identities further apart. However, despite their high accuracy in face recognition tasks, these NIR-based models remain susceptible to adversarial attacks.

### 2.2. Digital Adversarial Attacks

Adversarial attacks can be divided into white-box attacks and black-box attacks. In the white-box setting, where attackers have complete knowledge of the model’s structure and parameters, attacks are performed using optimization techniques, such as Box-constrained L-BFGS [30], C&W [2], *etc.* PGD [23] is a multi-step iterative method that uses

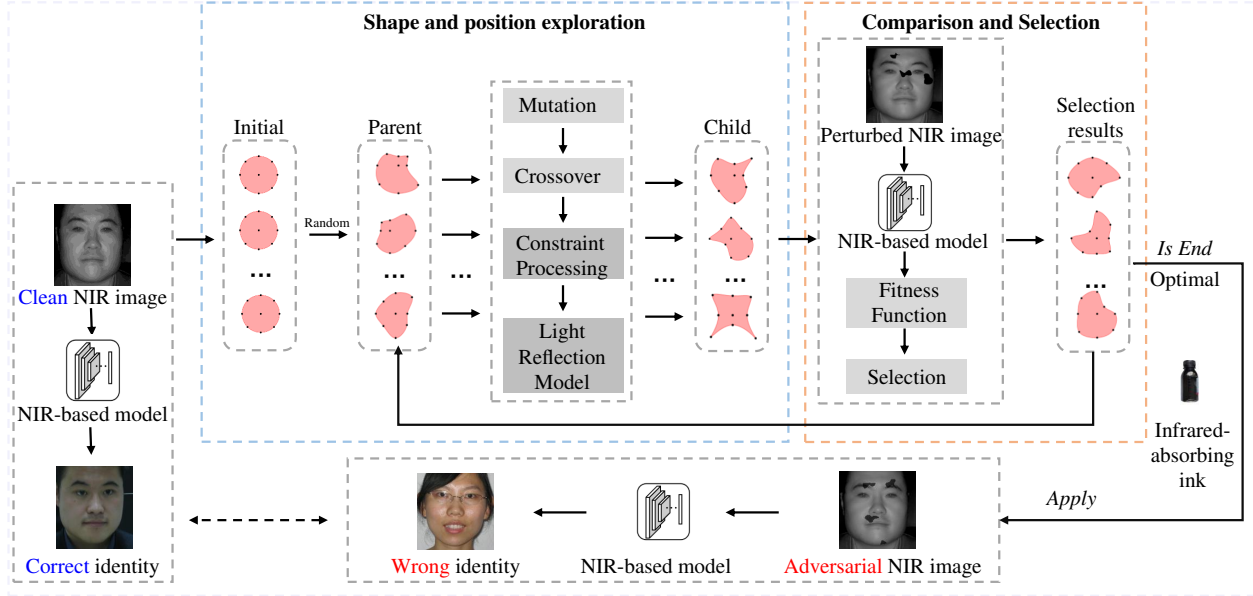


Figure 2. An overview of generating NIR face recognition adversarial patches using the Differential Evolution (DE) framework: The process starts with an initial population of shapes, which undergo shape and position exploration to generate a child population. A fitness function evaluates both parent and child populations, selecting the best individuals to enhance adversarial effectiveness. Finally, the optimal individual is then applied to the NIR image for the attack.

projected gradient descent on the negative loss function to generate adversarial examples. In contrast, black-box attacks do not require detailed model parameters and can be divided into three categories: transfer-based, score-based, and decision-based. For transfer-based methods, adversarial examples generated for one model can be transferred to another model, leading to successful attacks [9, 22, 5]. Score-based methods, where the target model’s predicted labels and probabilities are accessible, often employ gradient estimation [4] and random search [8]. Decision-based methods are more suitable for restrictive scenarios since only the model decisions are available [31]. Dong *et al.* [10] perform digital attacks on face recognition systems in this setting, modeling the local geometry of solution directions to improve efficiency. Attacks aimed at changing the predicted class from the true label are referred to as untargeted attacks (dodging), while attacks targeting a specific class are known as targeted attacks (impersonation). Although digital attacks expose model vulnerabilities, they often fail in real-world scenarios due to physical constraints.

### 2.3. Physical Adversarial Attacks

Existing physical attacks on VIS face recognition are divided into printed and light methods. Printed-based adversarial attacks embed perturbation patterns within fixed regions of commonplace accessories such as hats [17], glasses [28], and masks [45], where adversarial optimization explicitly accounts for printer gamut constraints.

This compensates for color deviations between digital and physical reproductions, ensuring the realizability of attacks under real-world imaging conditions. However, the printed method inevitably generates visually conspicuous artifacts in adversarial patterns due to unconstrained color-space optimization. To achieve stealthy adversarial attacks, some studies utilize human-imperceptible optical phenomena (*e.g.*, invisible infrared light [33, 43], persistence of vision [29]) to interfere with captured RGB face images and successfully mislead the VIS face recognition model’s output. Although substantial research has focused on adversarial attacks against VIS face recognition systems, these methods have limited transferability to NIR systems due to NIR spectral filtering and lower dimensionality. To address this, research [6] minimizes NIR spectral color discrepancies between digital simulations and physical prints by employing color-constrained adversarial perturbation optimization, thus tackling the mismatch between digital and physical optimality. However, while this work proposes physical printable glasses attacks on NIR face recognition systems, it also introduces conspicuous artifacts in the VIS setting. To the best of our knowledge, no prior work has proposed human-imperceptible physical adversarial attacks for NIR face recognition systems.

## 3. Methodology

In this section, we first briefly introduce the target of adversarial attacks in face recognition, then describe our at-

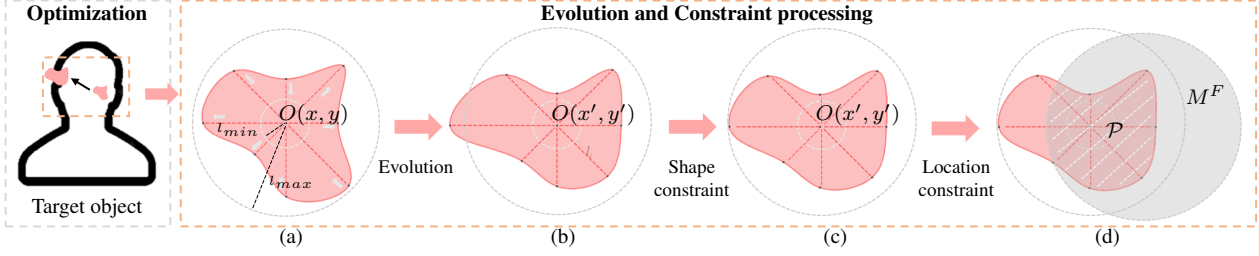


Figure 3. The shape and position optimization with constraint process is illustrated as follows: Subfigure (a) depicts the evolution of the shape and its position. Subfigure (b) shows the updated shape after the adjustment in (a), which exceeds the parameter boundaries. Subfigure (c) presents the corrected shape derived from (b). Finally, Subfigure (d) highlights the valid area, denoted as  $\mathcal{P}$ , constrained within  $M^F$ .

tack method for optimizing patches in the digital and physical domains.

### 3.1. Problem Formulation

In the NIR face recognition task, given a clean NIR image  $x^{nir}$ , the goal of the adversarial attack is to make the NIR face recognition model predict an incorrect identity of the perturbed image  $x_{adv}^{nir}$ . The adversarial multi-patch perturbation image can be generated using Eq. (1).

$$x_{adv}^{nir} = (1 - \mathcal{M}) \odot x^{nir} + \mathcal{M} \odot \hat{x}^{nir} \quad (1)$$

where  $\odot$  is the Hadamard product,  $\hat{x}^{nir}$  is the adversarial multi-patch, and  $\mathcal{M} \in \{0, 1\}^{h \times w}$  is a mask matrix to constrain the shape and position of the adversarial patch applied to the target object.

Particularly, there are two types of adversarial attacks on face recognition: dodging (untargeted) attacks and impersonation (targeted) attacks. Given the NIR face recognition model  $f(\cdot, \cdot)$ , ground-truth label  $\hat{t}$  for  $x^{nir}$  and  $x_{adv}^{nir}$ , the goal of a **dodging** attack is to find the optimal attack parameters  $\mathcal{P}_s^*$  to make the probability corresponding to the gallery VIS image  $x_t^{vis}$  as small as possible so that any person different from  $\hat{t}$  is regarded as the top-1 identity. So the objective function of the dodging attack can be formalized as:

$$\min_{\mathcal{P}_s} \mathcal{L}_{dodging}(\mathcal{P}_s) = f(x_{adv}^{nir}, x_t^{vis}) \quad (2)$$

For the **impersonation** attack, given a target identity  $t^*$ , the objective function is defined as follows, which aims to make the probability of the target label as the top-1 identity:

$$\min_{\mathcal{P}_s} \mathcal{L}_{impersonation}(\mathcal{P}_s) = 1 - f(x_{adv}^{nir}, x_{t^*}^{vis}) \quad (3)$$

### 3.2. Ink Shaping Attack in the Digital Domain

Previous methods have either focused on optimizing the content of adversarial patches [21] or their positions [44, 34], both of which suffer from limited stealthiness and poor effectiveness. Therefore, in this paper, we use location and

shape to model a patch and optimize both simultaneously, which significantly enhances the performance of the attack.

**Patch Location:** To improve the effectiveness of the attack, we employ a multi-patch joint attack strategy. Specifically, we first propose identifying a set of coordinates  $\mathcal{O}_s = \{(x_1, y_1), (x_2, y_2), \dots, (x_m, y_m)\}$  to control the central positions of patches  $\mathcal{P}_s = \{\mathcal{P}_1, \mathcal{P}_2, \dots, \mathcal{P}_m\}$ , where  $m$  is the number of patches. This can be formulated as follows:

$$\mathcal{O}_s = \{(x_i, y_i) \mid x_l \leq x_i \leq x_r, y_d \leq y_i \leq y_u \mid 0 \leq i < m\} \quad (4)$$

where  $x_l, x_r, y_d$ , and  $y_u$  denote the minimum and maximum bounds of the image's width and height.

Additionally, to determine the valid face mask  $M^F \in R^{h \times w}$  for applying patches (e.g., cheeks and forehead, etc., while excluding critical facial features like the eyes and mouth), we first extract the key facial feature points and then fill the effective region to generate the mask. Therefore, the final patch application areas  $\mathcal{M}$  are defined by  $\mathcal{P}_i \cap M^F$  for  $i = 1, 2, \dots, m$ .

**Patch Shape.** Most prior studies use a set of vertices to define a polygon [36, 42]. However, this approach will result in overlapping patch contours or excessively large patches. To address these issues, we propose a novel shape representation that implements radial distances and angles of each vertex. Given the number of vertex  $n$  and sets of radial distances  $\mathcal{L}_s = \{(l_{11}, l_{12}, \dots, l_{1n})(l_{21}, l_{22}, \dots, l_{2n}) \dots (l_{m1}, l_{m2}, \dots, l_{mn})\}$ , the coordinate  $(x_{p_{ij}}, y_{p_{ij}})$  of each  $j$ -th vertex for the  $i$ -th patch can be formulated by:

$$p_{ij} = \begin{cases} x_{p_{ij}} = x_i + l_{ij} \cdot \cos(j \cdot \theta) \\ y_{p_{ij}} = y_i + l_{ij} \cdot \sin(j \cdot \theta) \\ l_{\min} \leq l_{ij} \leq l_{\max} \end{cases} \quad (5)$$

where  $x_i, y_i$  represent the  $i$ -th patch's central position's coordinates,  $\theta = \frac{2\pi}{n}$  indicates the angular spacing between  $p_{ij}$  and  $p_{i,j+1}$ , and  $l_{\min}$  and  $l_{\max}$  impose constraints on the magnitude of deformations applied to the patch, making the patch appear as if the distortions were caused by camera capture errors.



To ensure the shape’s naturalness, we use the B-spline curve [7] to connect  $i$ -th patch’s each vertex to generate the patch contour  $M_i^{con}$  represented by:

$$M_i^{con} = \{Bspline(p_{ij-1}, p_{ij}, p_{ij+1}, p_{ij+2} | 0 \leq j < n\} \quad (6)$$

With  $M_i^{con}$  being closed, we can easily fill  $M_i^{con}$  and get the final  $i$ -th patch’s shape  $\mathcal{P}_i$ .

**Optimization Algorithm.** To launch the attack under black-box settings, we employ the Differential Evolution (DE) algorithm to optimize the patch, which efficiently explores the search space to find the optimum for Eq. (2) and Eq. (3). DE algorithm consists of four steps: starting from an initial population, using the crossover and mutation to generate the offspring population, making the fittest survive according to the fitness function, and finding the appropriate solution in the iterative evolution process.

In our case, a population represents a multi-patch attack strategy  $\mathcal{P}_s = \{\mathcal{P}_1, \mathcal{P}_2, \dots, \mathcal{P}_m\}$ . Given the population size  $Q$ , the  $k$ -th generation solutions  $S(k)$  are represented as:

$$S(k) = \{S_i(k) | \theta_j^L \leq S_{ij}(k) \leq \theta_j^U, 1 \leq i \leq Q, 1 \leq j \leq n\} \quad (7)$$

where  $S_i(k)$  is the shapes and positions of  $i$ -th multi-patch and  $S_{ij}(k)$  is the parameters of shapes (e.g.,  $\mathcal{L}_s$ ) and positions (e.g.,  $\mathcal{O}_s$ ). Here  $\theta_j^L$  and  $\theta_j^U$  together make up the multi-feasible regions  $\mathcal{M}_i$ , which are the allowable range of the shape and location parameters.

In the  $k + 1$  generation of DE, the solution  $S(k + 1)$  is achieved via crossover, mutation, and selection based on  $S(k)$ . A fitness function is applied on  $S_i(k)$  to evaluate its attack effectiveness. During this process, the fitness function solely relies on the confidence scores of each identity. Consequently, black-box attacks can be performed to find the optimal multi-patch attack solution  $\mathcal{P}_s^*$ . The shape evolution process is shown at Fig. 3.

### 3.3. Ink Shaping Attack in the Physical Domain

To generate robust adversarial examples in the physical domain, we implement the following method to minimize the gap between the digital domain and the physical domain:

**Light Reflection Model.** NIR images are formed by reflecting light from NIR LEDs off the skin, which makes the pixel values received by the NIR camera different from what we optimize in the digital world. To reduce this discrepancy, we model the light reflection equation as a BRDF function [26], which is represented by:

$$f(\mathbf{l}, \mathbf{v}) = D_d + \frac{D(\theta_h) F(\theta_d) G(\theta_l, \theta_v)}{4 \cos \theta_l \cos \theta_v} \quad (8)$$

where  $D_d$  is a diffuse component,  $D(\theta_h)$  is Beckmann Microfacet Distribution Function describing the distribution of

---

#### Algorithm 1: Shape Optimization for NIR Attack

---

**Input:** Network  $f$ , clean NIR image  $x^{nir}$  and label  $t$ , the fitness function  $\mathcal{J}(\cdot)$ , the objective function  $\mathcal{L}(\cdot)$ , population size  $P$ , max iteration number  $T$ , face region mask  $M^F$ , value ranges  $[l_{min}, l_{max}]$

**Output:** Adversarial NIR image  $x_{adv}^{nir}$

- 1 Initialize  $S(0)$  randomly in deformation and position constraints,  $\mathcal{J}(\cdot) = \mathcal{L}(\cdot)$
- 2 **for**  $k = 0$  to  $T - 1$  **do**
- 3     Sort  $S(k)$  in descending order based on  $\mathcal{J}(S(k))$
- 4     **if**  $S_0(k)$  makes the attack successful **then**
- 5          $stop = k$ ; **break**;
- 6     **end**
- 7     Generate  $S(k + 1)$  based on crossover and mutation
- 8     **for**  $i = 1$  to  $P$  **do**
- 9         Evaluate  $S_i(k)$ ,  $S_i(k + 1)$  according to  $\mathcal{J}(\cdot)$
- 9          $S_i(k + 1) \leftarrow$  the better one in  $S_i(k)$ ,  $S_i(k + 1)$
- 10    **end**
- 11 **end**
- 12 Sort  $S(stop)$  in descending order according to  $\mathcal{J}(\cdot)$
- 13  $Pos$  &  $Def$  parameters for  $\mathcal{P}_s^* \leftarrow S_0(stop)$
- 14 Calculate the each patches’ vertices by Eq. (5)
- 15  $M^{con} \leftarrow$  combine each patch’s vertices by Eq. (6)
- 16  $\mathcal{P}_s^* \leftarrow$  fill the  $M^{con}$
- 17  $\mathcal{M} \leftarrow$  restricts the perturbation region  $M^F \cap \mathcal{P}_s^*$
- 18  $x_{adv}^{nir} \leftarrow$  get final multi-patch by light reflection model
- 19 **return**  $x_{adv}^{nir}$

---

microfacets on a surface,  $F(\theta_d)$  is Fresnel Reflection equation approximating how much light is reflected at different angles and  $G(\theta_l, \theta_v)$  is Beckmann Geometry term accounting for the occlusion and shadowing effects that can occur during reflection. Specifically, given a NIR light intensity  $I$  and the original NIR image  $x_{orig}^{nir}$ , the adversarial NIR image  $x_{adv}^{nir}$  can be formulated by:

$$x_{adv}^{nir} = I \cdot f(\mathbf{l}, \mathbf{v}) \cdot x_{orig}^{nir} \quad (9)$$

The overall algorithm for generating adversarial patches is summarized in Algorithm 1, and the whole illustration for this framework is given in Fig. 2.

## 4. Experiments

This section begins by presenting the experimental setup and then compares our multi-patch adversarial attack with the state-of-the-art (SOTA) method proposed by Cohen and Sharif [6] in both the digital and physical domains.

### 4.1. Experiment Setup

**Datasets:** We conduct evaluations on three benchmark NIR-VIS datasets: the CASIA NIR-VIS 2.0 face database [20], the BUAA-VisNir face database [15], and the Oulu-CASIA NIR-VIS facial expression database [41]. The **CASIA NIR-VIS 2.0** with 725 subjects (1-22 VIS/5-50 NIR

Table 1. The results of attacks on the face recognition task. We report the attack success rate (ASR) of adversarial examples generated by our method and AiD [6] on the CASIA [20], BUAA [15], and Oulu-CASIA [41] datasets, evaluated against ResNeSt [40], LightCNN [38], LightCNN-DVG [12], and LightCNN-Rob [37]. The gray cells represent white-box attack results, while the white cells represent black-box attack results. The optimal black-box attack results are highlighted in bold.

Method	Target models		ResNeSt	LightCNN	DVG	Rob	ResNeSt	LightCNN	DVG	Rob
	Soure models									
CASIA			Dodging				Impersonation			
AiD	ResNeSt		97.64%	12.46%	0.00%	0.00%	27.87%	1.71%	0.00%	0.00%
AiD	LightCNN		39.35%	98.86%	82.91%	15.13%	1.57%	26.19%	17.81%	0.28%
AiD	DVG		37.96%	94.82%	96.21%	22.13%	1.42%	20.06%	25.07%	2.54%
AiD	Rob		36.55%	66.11%	56.16%	61.49%	1.26%	7.54%	10.66%	14.29%
Ours			89.29%	97.44%	84.85%	62.91%	76.96%	66.85%	33.01%	35.11%
BUAA			Dodging				Impersonation			
AiD	ResNeSt		99.26%	0.00%	0.00%	0.00%	100.00%	0.00%	0.00%	0.00%
AiD	LightCNN		26.53%	99.32 %	82.43%	25.85%	5.14%	98.64%	82.31%	14.48%
AiD	DVG		25.17%	96.59%	98.64%	38.09%	4.41%	87.76%	95.24%	20.69%
AiD	Rob		7.43%	27.21%	39.46%	80.69%	3.68%	19.04%	30.61%	78.23%
Ours			64.71%	91.16%	83.67%	42.76%	44.89%	40.14%	38.09%	32.43%
Oulu-CASIA			Dodging				Impersonation			
AiD	ResNeSt		89.33%	17.94%	20.51%	29.49%	90.82%	10.67%	11.54%	11.84%
AiD	LightCNN		26.92%	98.73%	84.62%	41.03%	13.33%	91.03%	79.49%	7.89%
AiD	DVG		17.95%	89.74%	91.03%	48.72%	10.67%	87.18%	92.31%	22.37%
AiD	Rob		19.74%	61.84%	63.16%	77.63%	8.00%	42.31%	56.41%	69.74%
Ours			72.00%	92.31%	89.74%	78.95%	58.67%	67.94%	65.38%	61.84%

images per subject) captured under visible light and 850nm NIR illumination, exhibiting pose, expression, and distance variations. The **BUAA-VisNir** contains 150 subjects with synchronized VIS-NIR pairs via multispectral imaging under controlled illumination gradients. And the **Oulu-CASIA** ([41]) features 80 subjects performing six expressions under three illuminations with 25fps video sequences. **Evaluation method:** We evaluate the proposed method by attacking the identification results from state-of-the-art NIR face recognition models, which includes ResNeSt [40], LightCNN [38], LightCNN-DVG [12], and LightCNN-Rob [37], all achieving 100% baseline identification accuracy under benign conditions. Attack Success Rate (ASR) is quantified through two critical metrics:

- **Dodging:** Aims to evaluate the method’s ability to evade correct recognition by suppressing the confidence score of the ground-truth identity, ensuring it is not selected as the system’s top-1 prediction.
- **Impersonation:** Aims to evaluate the method’s ability to force target recognition by increasing the target identity’s confidence score relative to others, ensuring it becomes the top-1 prediction.

We also benchmark against Accessorize in the Dark (AiD) [6], the current state-of-the-art (SOTA) physical attack on NIR face recognition systems, by comparing ASRs in both digital and physical domains, with experiments conducted by volunteers, as shown in Fig. 4.

**Implementation:** To determine the patch position, we use the `dlib` library to extract 81 facial feature points and fill the effective region to generate the mask  $M^F$ . The shape parameters for the attack are set as follows: the number of patches  $m$  is 4, the number of vertex  $n$  is 8, and the value range of shape deformation constraint  $[l_{\min}, l_{\max}] = [2, 20]$ . The optimization algorithm parameters are configured with a population size  $P = 40$ , and the maximum number of iterations  $T = 200$ .

## 4.2. Digital Domain Attacks

We first perform white-box and transfer-based black-box attacks using the AiD approach and compare their attack success rate (ASR) with our method in the black-box setting, which only relies on the models’ predicted labels and probabilities. The results are presented in Tab. 1. We first compare our black-box attacks with AiD’s transfer-based black-box attacks. In the black-box setting, our method attains an average ASR of 65.45% and 51.77% performing dodging and impersonation attacks, respectively, outperforming AiD’s average ASR of 37.61% and 19.30%. Although constrained by limited information, our method’s average ASR is only reduced by 13.64% compared to the white-box AiD attacks, which have complete knowledge of the model’s structure and parameters. Additionally, four groups of visual examples are shown in Fig. 5. As observed, our method effectively decreases the probability of the ground-truth identity, ensuring that the probabilities of others exceed it, thus achieving a successful attack with

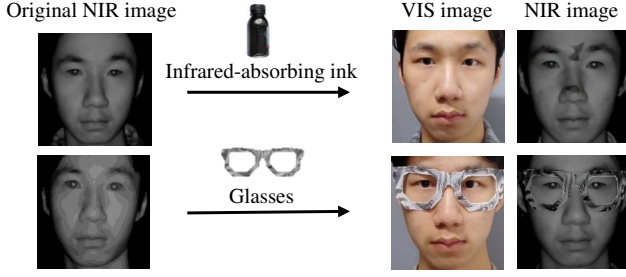


Figure 4. Experiment preparation for our method and AiD [6]

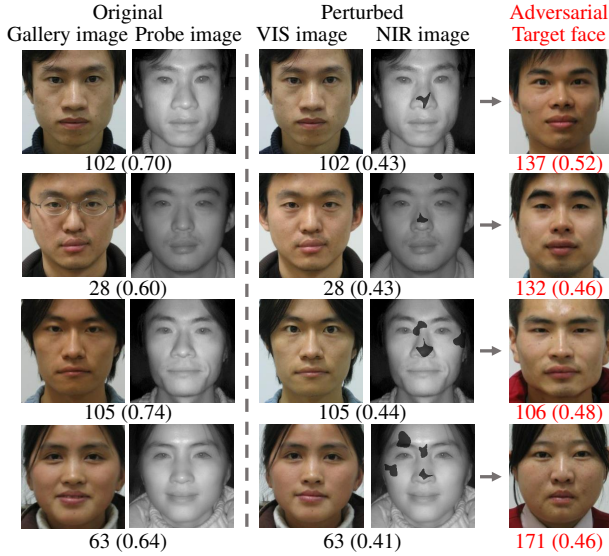


Figure 5. Examples of digital attacks using ink-shaping attack. For each group, the five images correspond to the gallery VIS image, the unattacked original image, the VIS and NIR image after the attacks, and the VIS image corresponding to the predicted wrong class after the attacks. Black text denotes the original correct ID and its probability, while red text indicates the misclassified ID and its confidence after the attack.

minimal attention. These findings highlight that our method achieves more effective attacks across various network architectures compared to the SOTA method (AiD) in the digital domain.

### 4.3. Physical Domain attacks

Here we utilize three methods to implement physical attacks: ours, AiD, and random. We first optimize the patches’s parameters using the front-facing NIR image in the digital domain by our method and AiD, then perform attacks in the physical domain, as shown in Fig. 4. Additionally, random method attacks are triggered by the stochastic application of infrared-absorbing ink to various areas of the facial regions. Following [35], we recorded a 35-second video at 10 frames per second (approximately 350 frames in total), capturing NIR images with adversarial per-

Table 2. The percentage of video frames successfully attacked when continuously changing face postures in the physical domain.

Models	ResNeSt	LightCNN	DVG	Rob
Ours	95.42%	83.49%	80.05%	70.82%
AiD	100.00%	55.44%	22.54%	78.74%
Random	90.91%	28.86%	13.89%	50.28%

Table 3. The probabilities of the ground-truth label 0 before and after the attack in the physical domain.

Models	ResNeSt	LightCNN	DVG	Rob
Dodging				
Attack type				
Before-attack	1.00	0.59	0.74	0.55
After-attack	0.32	0.38	0.36	0.36
Difference(↓)	0.68	0.11	0.38	0.19
Impersonation				
Attack type				
Before-attack	1.00	0.99	1.00	0.55
After-attack	0.26	0.27	0.33	0.23
Difference(↓)	0.74	0.72	0.67	0.22

turbations under varying face postures (e.g., front-facing, upward gaze, and rotations within a 30-degree range), as shown in Fig. 6. As observed, our approach achieved successful attacks across various face postures while introducing minor perturbations in the perturbed NIR images and remaining human-imperceptible in the perturbed VIS images. The quantitative results are shown in Tab. 2. The average ASR of our method is 82.46%, significantly outperforming the AiD method (64.18%) and the random method (45.84%). This superiority stems from optimizing shape and position, which, unlike color optimization, are more robust in physical attack scenarios as they remain relatively stable in real-world conditions. Moreover, the results also confirm that only optimized shapes and positions can exploit model vulnerabilities and effectively execute physical attacks. Additionally, we compute the percentage of frames under different face postures, as shown in Fig. 7 (a). Our method demonstrates superior robustness in maintaining attack effectiveness across different face postures, outperforming both AiD and the random method, except under extreme deformations or near-invisibility. This highlights the effectiveness of our attack framework in addressing the optimization mismatch between digital and real-world domains, ultimately leading the patch toward its physically optimal shape and position. Furthermore, we also conduct dodging and impersonation attacks in the physical domain. As shown in Tab. 3, the ground-truth labels’ probabilities in different models are significantly reduced, which proves that the generated attack parameters in the digital domain can still maintain a good attack performance when applied to the physical domain.

## 5. Ablation Study

This section presents ablation studies to assess the impact of various factors on optimizing adversarial patch at-

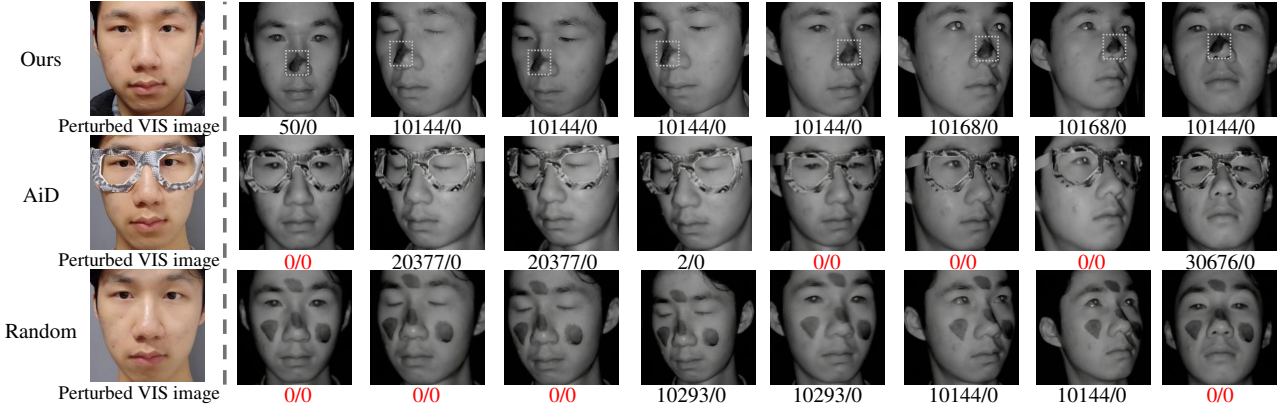


Figure 6. The examples demonstrate physical attacks on NIR face recognition models. They present VIS images perturbed with infrared-absorbing ink or glasses and evaluate attack effectiveness across different facial postures using our method, AiD [6], and random method. The text below each image displays the predicted and ground-truth labels, with failed attacks highlighted in red. The perturbed ink areas are highlighted by white rectangular boxes.

tacks, including position and shape optimization and the Light Reflection Model strategy.

### 5.1. Effects of Position and Shape Optimization

To investigate the effects of our optimized positional attributes, we randomly select several positions for subsequent shape-only optimization; To examine the influence of shape optimization, we first generate adversarial multi-patches to determine the optimal positions for a given sample and then alter the optimal shapes to basic forms such as circles, squares, rectangles, and triangles. The results are presented in Tab. 4. The combined shape and position optimization method achieves an average ASR of 83.25%, outperforming the shape-only optimization by 66.07% and the position-only optimization by 63.34%. These findings highlight the critical role of shape and position attributes in enhancing the effectiveness of our adversarial attacks.

Table 4. The ASR comparison with different optimization attributes for dodging attack across various models.

Opt. attributes	Shape + Position	Shape	Position
ResNeSt	<b>72.00%</b>	4.00%	18.39%
LightCNN	<b>92.31%</b>	17.95%	14.36%
DVG	<b>89.74%</b>	23.08%	12.05%
Rob	<b>78.95%</b>	23.68%	34.87%

### 5.2. Effects of Light Reflection Model Strategy

Considering the imaging differences between the digital and physical domains, we propose a Light Reflection Model (LRM) to generate more effective shapes. To evaluate the effectiveness of the LRM, we optimized our patch both with and without the LRM. When using the LRM, we followed the method proposed in Sec. 3.3 to generate the adversarial NIR image. In the absence of the LRM, we simply set the

Table 5. The percentage of video frames successfully attacked optimization with or without LRM strategy in the physical domain.

Optimization methods	w/ LRM	w/o LRM	Difference
ResNeSt	94.86%	84.38%	↓10.48%
LightCNN	83.49%	18.50%	↓64.99%
DVG	80.05%	26.37%	↓53.68%
Rob	70.82%	49.54%	↓21.28%

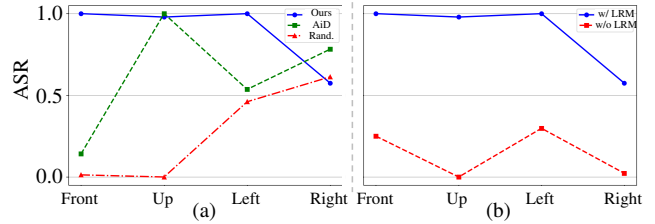


Figure 7. The comparison of attack success rates across different face postures. Subfigure (a) compares three physical attack methods: Ours, AiD, and Rand. Subfigure (b) compares the optimal results of our approach under two conditions: with and without LRM.

pixel values of the patch region to zero. The quantitative results, presented in Tab. 5, indicate a 37.61% increase in the average ASR with LRM strategy, compared to its absence. Furthermore, we calculate the percentage of successful attack frames across various face postures in the physical domain, as shown in Fig. 7 (b). The experimental validation confirms the crucial role of LRM in achieving the posture robustness of our patch, since without LRM optimization, the ASR dropped sharply by more than 90% in both upward and rightward poses. These results highlight the critical role of LRM in achieving physically optimal adversarial patch attacks.



## 6. Limitation

In this study, we focused on adversarial patch attacks targeting NIR face recognition systems equipped with 850 nm wavelength filters, as they are widely used. However, the presence of NIR cameras operating at different wavelengths (e.g., 810 nm, 850 nm) can lead to variations in imaging characteristics, potentially affecting our patch's performance. In future work, we will explore the development of more generalized adversarial patches capable of operating across a broader range of wavelengths. This would involve testing and optimizing patches for various NIR wavelength filters, including 810 nm, 850 nm, and others, to enhance the robustness of attacks across diverse camera setups.

## 7. Conclusion

In this paper, we propose a novel human-imperceptible physical adversarial attack against NIR face recognition models, emphasizing the security risks of these systems in real-world deployments. By leveraging infrared-absorbing ink, we design a stealthy adversarial patch that disrupts NIR imaging while remaining visually inconspicuous. Our method optimizes both the shape and position of adversarial patches using a differential evolution algorithm and further enhances transferability from digital to physical domains through a light reflection model. Experimental results demonstrate that our approach achieves significantly higher ASR than the SOTA method. These findings highlight the vulnerability of NIR face recognition systems and underscore the need for more robust defense mechanisms.

## References

- [1] Apple. *Apple Platform Security*, 2023. Available at [https://help.apple.com/pdf/security/en\\_US/apple-platformsecurity-guide.pdf](https://help.apple.com/pdf/security/en_US/apple-platformsecurity-guide.pdf). 1, 2
- [2] Nicholas Carlini and David Wagner. Towards evaluating the robustness of neural networks. In *2017 IEEE Symposium on Security and Privacy (SP)*, pages 39–57. IEEE, 2017. 2
- [3] Laura Rodríguez Carlos-Roca, Isabelle Hupont Torres, and Carles Fernández Tena. Facial recognition application for border control. In *2018 International Joint Conference on Neural Networks (IJCNN)*, pages 1–7. IEEE, 2018. 1
- [4] Pin-Yu Chen, Huan Zhang, Yash Sharma, Jinfeng Yi, and Cho-Jui Hsieh. Zoo: Zeroth order optimization based black-box attacks to deep neural networks without training substitute models. In *Proceedings of the 10th ACM Workshop on Artificial Intelligence and Security*, pages 15–26, 2017. 3
- [5] Sizhe Chen, Zhengbao He, Chengjin Sun, Jie Yang, and Xiaolin Huang. Universal adversarial attack on attention and the resulting dataset damagenet. *IEEE Transactions on Pattern Analysis and Machine Intelligence*, 44(4):2188–2197, 2020. 3
- [6] Amit Cohen and Mahmood Sharif. Accessorize in the dark: A security analysis of near-infrared face recognition. In *European Symposium on Research in Computer Security*, pages 43–61. Springer, 2023. 2, 3, 5, 6, 7, 8
- [7] Maurice G Cox. The numerical evaluation of b-splines. *IMA Journal of Applied Mathematics*, 10(2):134–149, 1972. 5
- [8] Francesco Croce, Maksym Andriushchenko, Naman D Singh, Nicolas Flammarion, and Matthias Hein. Sparse-rs: a versatile framework for query-efficient sparse black-box adversarial attacks. In *Proceedings of the AAAI Conference on Artificial Intelligence*, volume 36, pages 6437–6445, 2022. 3
- [9] Yinpeng Dong, Fangzhou Liao, Tianyu Pang, Hang Su, Jun Zhu, Xiaolin Hu, and Jianguo Li. Boosting adversarial attacks with momentum. In *Proceedings of the IEEE conference on computer vision and pattern recognition*, pages 9185–9193, 2018. 3
- [10] Yinpeng Dong, Hang Su, Baoyuan Wu, Zhifeng Li, Wei Liu, Tong Zhang, and Jun Zhu. Efficient decision-based black-box adversarial attacks on face recognition. In *proceedings of the IEEE/CVF conference on computer vision and pattern recognition*, pages 7714–7722, 2019. 3
- [11] Chaoyou Fu, Xiang Wu, Yibo Hu, Huaibo Huang, and Ran He. Dual variational generation for low shot heterogeneous face recognition. *Advances in neural information processing systems*, 32, 2019. 2
- [12] Chaoyou Fu, Xiang Wu, Yibo Hu, Huaibo Huang, and Ran He. Dvg-face: Dual variational generation for heterogeneous face recognition. *IEEE transactions on pattern analysis and machine intelligence*, 44(6):2938–2952, 2021. 1, 2, 6
- [13] Shuowen Hu, Nathaniel Short, Benjamin S Riggan, Matthew Chasse, and M Saquib Sarfraz. Heterogeneous face recognition: recent advances in infrared-to-visible matching. In *2017 12th IEEE International Conference on Automatic Face & Gesture Recognition (FG 2017)*, pages 883–890. IEEE, 2017. 2
- [14] Weipeng Hu, Wenjun Yan, and Haifeng Hu. Dual face alignment learning network for nir-vis face recognition. *IEEE Transactions on Circuits and Systems for Video Technology*, 32(4):2411–2424, 2021. 2
- [15] D Huang, Jia Sun, and Y Wang. The buaa-visnir face database instructions. *School Comput. Sci. Eng., Beihang Univ., Beijing, China, Tech. Rep. IRIP-TR-12-FR-001*, 3(3):8, 2012. 5, 6
- [16] Fangling Jiang, Pengcheng Liu, and Xiangdong Zhou. Multilevel fusing paired visible light and near-infrared spectral images for face anti-spoofing. *Pattern recognition letters*, 128:30–37, 2019. 2
- [17] Stepan Komkov and Aleksandr Petiushko. Advhat: Real-world adversarial attack on arcface face id system. In *2020 25th international conference on pattern recognition (ICPR)*, pages 819–826. IEEE, 2021. 3
- [18] Seong G Kong, Jingu Heo, Besma R Abidi, Joonki Paik, and Mongi A Abidi. Recent advances in visual and infrared face recognition—a review. *Computer vision and image understanding*, 97(1):103–135, 2005. 1
- [19] Anoop Krishnan, Brian Neas, and Ajita Rattani. Is facial recognition biased at near-infrared spectrum as well? In *2022 IEEE International Symposium on Technologies for Homeland Security (HST)*, pages 1–7. IEEE, 2022. 1

- [20] Stan Li, Dong Yi, Zhen Lei, and Shengcai Liao. The casia nir-vis 2.0 face database. In *Proceedings of the IEEE conference on computer vision and pattern recognition workshops*, pages 348–353, 2013. 5, 6
- [21] Xin Liu, Huanrui Yang, Ziwei Liu, Linghao Song, Hai Li, and Yiran Chen. Dpatch: An adversarial patch attack on object detectors. *arXiv preprint arXiv:1806.02299*, 2018. 4
- [22] Yanpei Liu, Xinyun Chen, Chang Liu, and Dawn Song. Delving into transferable adversarial examples and black-box attacks. *arXiv preprint arXiv:1611.02770*, 2016. 3
- [23] Aleksander Madry. Towards deep learning models resistant to adversarial attacks. *arXiv preprint arXiv:1706.06083*, 2017. 2
- [24] Yunqi Miao, Alexandros Lattas, Jiankang Deng, Jungong Han, and Stefanos Zafeiriou. Physically-based face rendering for nir-vis face recognition. *Advances in Neural Information Processing Systems*, 35:22752–22764, 2022. 2
- [25] Microsoft. *Windows Hello for Business Overview*, 2023. Available at <https://docs.microsoft.com/en-us/windows/security/identityprotection/hello-for-business/hello-overview>. 1, 2
- [26] Gabriela Schaepman-Strub, Michael E Schaepman, Thomas H Painter, Stefan Dangel, and John V Martonchik. Reflectance quantities in optical remote sensing—definitions and case studies. *Remote sensing of environment*, 103(1):27–42, 2006. 5
- [27] Adi Shamir, Itay Safran, Eyal Ronen, and Orr Dunkelman. A simple explanation for the existence of adversarial examples with small hamming distance, 2019. 2
- [28] Mahmood Sharif, Sruti Bhagavatula, Lujo Bauer, and Michael K Reiter. Accessorize to a crime: Real and stealthy attacks on state-of-the-art face recognition. In *Proceedings of the 2016 acm sigsac conference on computer and communications security*, pages 1528–1540, 2016. 1, 3
- [29] Meng Shen, Zelin Liao, Liehuang Zhu, Ke Xu, and Xiaojiang Du. Vla: A practical visible light-based attack on face recognition systems in physical world. *Proceedings of the ACM on Interactive, Mobile, Wearable and Ubiquitous Technologies*, 3(3):1–19, 2019. 2, 3
- [30] C Szegedy. Intriguing properties of neural networks. *arXiv preprint arXiv:1312.6199*, 2013. 1, 2
- [31] Guanhong Tao, Shengwei An, Siyuan Cheng, Guangyu Shen, and Xiangyu Zhang. Hard-label black-box universal adversarial patch attack. In *32nd USENIX Security Symposium (USENIX Security 23)*, pages 697–714, 2023. 3
- [32] Ya Wang, Tianlong Bao, Chunhui Ding, and Ming Zhu. Face recognition in real-world surveillance videos with deep learning method. In *2017 2nd international conference on image, vision and computing (icivc)*, pages 239–243. IEEE, 2017. 1
- [33] Ye Wang, Zeyan Liu, Bo Luo, Rongqing Hui, and Fengjun Li. The invisible polyjuice potion: An effective physical adversarial attack against face recognition. 1, 3
- [34] Hui Wei, Zhixiang Wang, Xuemei Jia, Yinqiang Zheng, Hao Tang, Shin’ichi Satoh, and Zheng Wang. Hotcold block: Fooling thermal infrared detectors with a novel wearable design. In *Proceedings of the AAAI conference on artificial intelligence*, volume 37, pages 15233–15241, 2023. 4
- [35] Xingxing Wei, Ying Guo, and Jie Yu. Adversarial sticker: A stealthy attack method in the physical world. *IEEE Transactions on Pattern Analysis and Machine Intelligence*, 45(3):2711–2725, 2022. 7
- [36] Xingxing Wei, Yao Huang, Yitong Sun, and Jie Yu. Unified adversarial patch for cross-modal attacks in the physical world. In *Proceedings of the IEEE/CVF International Conference on Computer Vision*, pages 4445–4454, 2023. 4
- [37] Tong Wu, Liang Tong, and Yevgeniy Vorobeychik. Defending against physically realizable attacks on image classification. *arXiv preprint arXiv:1909.09552*, 2019. 6
- [38] Xiang Wu, Ran He, Zhenan Sun, and Tieniu Tan. A light cnn for deep face representation with noisy labels. *IEEE transactions on information forensics and security*, 13(11):2884–2896, 2018. 1, 2, 6
- [39] Aijing Yu, Haoxue Wu, Huaibo Huang, Zhen Lei, and Ran He. Lamp-hq: A large-scale multi-pose high-quality database and benchmark for nir-vis face recognition. *International Journal of Computer Vision*, 129(5):1467–1483, 2021. 2
- [40] Hang Zhang, Chongruo Wu, Zhongyue Zhang, Yi Zhu, Haibin Lin, Zhi Zhang, Yue Sun, Tong He, Jonas Mueller, R Manmatha, et al. Resnest: Split-attention networks. In *Proceedings of the IEEE/CVF conference on computer vision and pattern recognition*, pages 2736–2746, 2022. 6
- [41] Guoying Zhao, Xiaohua Huang, Matti Taini, Stan Z Li, and Matti Pietikäläinen. Facial expression recognition from near-infrared videos. *Image and vision computing*, 29(9):607–619, 2011. 5, 6
- [42] Yiqi Zhong, Xianming Liu, Deming Zhai, Junjun Jiang, and Xiangyang Ji. Shadows can be dangerous: Stealthy and effective physical-world adversarial attack by natural phenomenon. In *Proceedings of the IEEE/CVF Conference on Computer Vision and Pattern Recognition*, pages 15345–15354, 2022. 4
- [43] Zhe Zhou, Di Tang, Xiaofeng Wang, Weili Han, Xiangyu Liu, and Kehuan Zhang. Invisible mask: Practical attacks on face recognition with infrared. *arXiv preprint arXiv:1803.04683*, 2018. 3
- [44] Xiaopei Zhu, Xiao Li, Jianmin Li, Zheyao Wang, and Xiaolin Hu. Fooling thermal infrared pedestrian detectors in real world using small bulbs. In *Proceedings of the AAAI conference on artificial intelligence*, volume 35, pages 3616–3624, 2021. 4
- [45] Alon Zolfi, Shai Avidan, Yuval Elovici, and Asaf Shabtai. Adversarial mask: Real-world universal adversarial attack on face recognition models. In *Joint European Conference on Machine Learning and Knowledge Discovery in Databases*, pages 304–320. Springer, 2022. 1, 3